Photon kinetic modeling of laser pulse propagation in underdense plasma

A. J. W. Reitsma
Department of Physics, University of Strathclyde, Glasgow G4 0NG, United Kingdom

R. M. G. M. Trines
Rutherford Appleton Laboratory, Chilton, Didcot, Oxon OX11 0QX, United Kingdom

R. Bingham
Rutherford Appleton Laboratory, Chilton, Didcot, Oxon OX11 0QX, United Kingdom
and Department of Physics, University of Strathclyde, Glasgow G4 0NG, United Kingdom

R. A. Cairns
School of Mathematics and Statistics, University of St. Andrews, Fife KY16 9SS, United Kingdom

J. T. Mendonça
Rutherford Appleton Laboratory, Chilton, Didcot, Oxon OX11 0QX, United Kingdom
and GOLP/Centro de Fisica de Plasmas, Instituto Superior Tecnico, 1096 Lisboa Codex, Portugal

D. A. Jaroszynski
Department of Physics, University of Strathclyde, Glasgow G4 0NG, United Kingdom

(Received 10 July 2006; accepted 29 September 2006; published online 9 November 2006)

This paper discusses photon kinetic theory, which is a description of the electromagnetic field in terms of classical particles in coordinate and wave number phase space. Photon kinetic theory is applied to the interaction of laser pulses with underdense plasma and the transfer of energy and momentum between the laser pulse and the plasma is described in photon kinetic terms. A comparison is made between a one-dimensional full wave and a photon kinetic code for the same laser and plasma parameters. This shows that the photon kinetic simulations accurately reproduce the pulse envelope evolution for photon frequencies down to the plasma frequency.
 [DOI: 10.1063/1.2366577]

I. INTRODUCTION

Due to recent technological advances, it is now possible to induce relativistic particle motion in the electromagnetic fields of a short pulse, high intensity laser. The light pressure of ultrashort laser pulses induces charge separation in a plasma and excites electric fields that are three to four orders of magnitude stronger[1] than those of conventional particle accelerators. This makes the interaction of intense laser pulses with plasma attractive for particle acceleration,[2] nuclear reactions,[3] and short wavelength radiation sources.[4] The evolution of a laser pulse as it interacts with a relativistic plasma is a complex process, as the plasma is a dielectric medium with a strongly nonlinear response to the laser fields, which induces feedback to the laser pulse due to spatial and temporal permittivity variations.[5] Understanding how to harness the plasma is fundamental to developing new technology from the laser-plasma interaction.

In this paper we discuss *photon kinetic theory*, a relatively novel method of describing the propagation of short laser pulses in underdense plasma. Photon kinetic theory is an example of a *wave kinetic theory*,[6] which elegantly describes the coupling of waves with very different time scales by representing the "fast" component of the wave by quasiparticles in the position-wave number phase space. The phase space representation is a natural way of dividing the time scales, as the evolution of the wave number coordinates corresponds to the spectral changes of the fast wave and the spatial evolution corresponds to the envelope changes, which are assumed to be "slow" and lead to coupling between the fast and slow waves. In the case of a laser pulse propagation in underdense plasma, the fast wave corresponds to the laser light pulse with a carrier frequency ω_0 and the slow wave is the plasma wave with plasma frequency $\omega_p \ll \omega_0$.

We formally convert the time amplitude representation of the electromagnetic field to position-wave number phase space of quasiparticles by a Wigner transform. The first physical applications of this transform are found in quantum mechanics studies in the 1930s.[7,8] However, the transform is well suited to describe classical wave-wave interactions. The development of photon kinetic formalism has been outlined in Ref. 9 and also in Ref. 10. Because the spectral and spatial content is separated in wave kinetic theories, they are inherently suitable for describing ultrashort pulse phenomena and broadband turbulence. For a laser pulse propagating in underdense plasma, the advantage of the photon kinetic description over the usual particle-in-cell method[11] is that a full resolution of the optical frequency and wavelength are not required. This leads to much faster and more efficient numerical codes, which allow larger propagation distances to be simulated and large parameter studies to be undertaken. Furthermore, the phase space representation inherent in the photon kinetic codes give additional insights into the evolution of the fields, as will be demonstrated in the simulation results presented in this paper. The price to pay for the enhanced efficiency is the loss of the phase of the electromag-

netic field in the photon kinetic description, which has the consequence of excluding a class of phase-dependent phenomena such as Raman backscattering.[12] However, other well known nonlinear laser-plasma instabilities, such as self-modulation,[13] self-focusing,[14] and filamentation,[15] are well described.

In this paper, we illustrate the power of the photon-kinetic approach to modeling laser-plasma interactions by comparing the predictions of a one-dimensional photon kinetic code with that of a full wave code. In both cases the laser-plasma interaction is described fully self-consistently using a relativistic cold fluid model to describe the plasma. To investigate two different important laser-plasma interaction regimes widely studied for electron acceleration,[16] we consider the case of an initial Gaussian laser pulse with a length much longer than the plasma wavelength, and compare this with the case of laser pulse duration equal to half a plasma wavelength. The short pulse resonantly excites a trailing plasma wave or *wakefield*, while the long pulse evolution is subject to the self-modulation instability. When the long pulse starts interacting with the plasma, it initially does not excite a trailing plasma wave. However, the self-modulation instability grows slowly and eventually excites large amplitude wakefields to the point where the plasma wave breaks, which results in trapping from the background plasma and subsequent acceleration of electrons. This process is known as *self-modulated* laser wakefield acceleration. In contrast, the evolution of the short pulse immediately drives a wakefield, and is thus useful for trapping externally injected electrons, which has the potential of controlling the acceleration process. This process is known as *resonant* laser wakefield acceleration. In this scenario, electron trapping from the background plasma is regarded as a source of *dark current*, i.e., an unwanted stream of particles with properties that cannot be controlled. Electron trapping from the background plasma and acceleration are excluded from our simulations due to the use of a fluid model for the plasma response. However, the purpose of our paper is to compare the photon kinetic model with the full wave model of laser pulse evolution. Electron trapping can be studied separately using a more complete model for the plasma response.

The paper is organized as follows: in Sec. II, the full wave equation is used to derive conservation laws that describe the conservation of wave action and the energy and momentum transfer between the laser and the plasma. In Sec. III we briefly describe the fluid model that we use for the plasma dynamics. In Sec. IV, we present a derivation of the photon kinetic equations and we show how the conservation laws outlined in Sec. II are reproduced. In Sec. V, the full wave and photon kinetic codes are described and simulation results are presented. Finally, Sec. VI is devoted to discussion and conclusions.

II. FULL WAVE THEORY

The starting point of our analysis is the following one-dimensional wave equation:[17]

$$\left[\frac{\partial^2}{\partial t^2}-\frac{\partial^2}{\partial z^2}+\Omega_p^2(z,t)\right]A(z,t)=0. \tag{1}$$

In this equation, A is a complex representation of the transverse vector potential that describes a circularly polarized laser pulse that propagates in a plasma. The quantity Ω_p is a generalized space and time-varying plasma frequency, which takes into account local ponderomotive and relativistic effects, as will be explained in Sec. III. For now, it is important to remark that Ω_p^2 is a real-valued quantity. Throughout this paper, we use a notation based on the convention $\hbar=m_e=c=1$, which explains why time and space are of the same dimensionality in Eq. (1).

From Eq. (1) it is not difficult to derive conservation laws for wave action, energy, and momentum. The conservation of the wave action,

$$\frac{\partial}{\partial t}\left[\frac{i}{2}\left(A\frac{\partial A^*}{\partial t}-A^*\frac{\partial A}{\partial t}\right)\right]+\frac{\partial}{\partial z}\left[\frac{i}{2}\left(A^*\frac{\partial A}{\partial z}-A\frac{\partial A^*}{\partial z}\right)\right]=0, \tag{2}$$

here written in the form of a continuity equation, follows directly from the property that Ω_p^2 is real-valued (the asterisk indicates a complex conjugate). As will become apparent in Sec. IV, a natural interpretation for the first quantity in square brackets is photon number density, and likewise the second quantity is interpreted as photon flux. Thus Eq. (2) establishes the important result that the number of photons is conserved for laser-plasma interaction as long as Ω_p^2 is real-valued.

Energy conservation is given by

$$\frac{\partial}{\partial t}\left[\frac{1}{2}\left(\frac{\partial A}{\partial t}\frac{\partial A^*}{\partial t}+\frac{\partial A}{\partial z}\frac{\partial A^*}{\partial z}+\Omega_p^2AA^*\right)\right]+\frac{\partial}{\partial z}\left[-\frac{1}{2}\left(\frac{\partial A}{\partial t}\frac{\partial A^*}{\partial z}+\frac{\partial A^*}{\partial t}\frac{\partial A}{\partial z}\right)\right]=\frac{1}{2}\frac{\partial\Omega_p^2}{\partial t}AA^*, \tag{3}$$

while momentum conservation is expressed as

$$\frac{\partial}{\partial t}\left[-\frac{1}{2}\left(\frac{\partial A}{\partial t}\frac{\partial A^*}{\partial z}+\frac{\partial A^*}{\partial t}\frac{\partial A}{\partial z}\right)\right]+\frac{\partial}{\partial z}\left[\frac{1}{2}\left(\frac{\partial A}{\partial t}\frac{\partial A^*}{\partial t}+\frac{\partial A}{\partial z}\frac{\partial A^*}{\partial z}-\Omega_p^2AA^*\right)\right]=-\frac{1}{2}\frac{\partial\Omega_p^2}{\partial z}AA^*. \tag{4}$$

The terms in the square brackets in these two equations denote the density and flux of energy and momentum carried by the electromagnetic field, with additional contributions from the $\Omega_p^2AA^*$ term. There are good reasons for including these contributions on the l.h.s. of the equations, as will become apparent in Sec. IV. Strictly speaking, Eqs. (3) and (4) are not conservation laws, as the r.h.s. is not generally equal to 0. As will be shown in Sec. III, the r.h.s. will reduce to 0 when we add the energy and momentum balance of the plasma to the model. Equations (3) and (4) demonstrate that the condition for energy and momentum exchange between the laser pulse and the plasma is that Ω_p^2 varies, respectively, temporally and spatially.

III. FLUID MODEL

From Sec. II it is apparent that a self-consistent description of laser-plasma interaction requires a model for the plasma response. In this section, we briefly describe the widely used relativistic cold fluid model in the quasistatic approximation.[18] The plasma ions are treated as an immobile neutralizing background with density n_0, which we use to define the ambient plasma frequency ω_p according to $\omega_p^2=4\pi n_0 e^2/m_e$ (in CGS units). The continuity equation for the plasma electron density $n(z,t)$ is

$$\frac{\partial n}{\partial t}+\frac{\partial(nv_z)}{\partial z}=0, \tag{5}$$

where $v_z=p_z/\gamma$ is the velocity, $p_z(z,t)$ is the longitudinal momentum, and $\gamma(z,t)$ is the Lorentz factor, which contains a contribution from the quiver motion in the laser field

$$\gamma^2=1+p_z^2+AA^*, \tag{6}$$

as follows from identifying the perpendicular momentum $\mathbf{p}_\perp$ with the vector potential $\mathbf{A}_\perp$. The $\Omega_p^2AA^*$ term in Eqs. (3) and (4) can now be identified as the energy associated with the quiver motion.

The equation for the longitudinal momentum is

$$\frac{\partial p_z}{\partial t}=\frac{\partial\phi}{\partial z}-\frac{\partial\gamma}{\partial z}, \tag{7}$$

where ϕ denotes the electrostatic potential. The second term on the r.h.s. of Eq. (7) represents the ponderomotive force, while the first term is the electrostatic field associated with plasma waves. The fluid model is completed with Poisson's equation

$$\frac{\partial^2\phi}{\partial z^2}=n-n_0. \tag{8}$$

In terms of this fluid model, the generalized plasma frequency is expressed as

$$\Omega_p^2=\frac{\omega_p^2 n}{\gamma n_0}, \tag{9}$$

so that energy and momentum exchange between laser pulse and plasma are seen to arise from relativistic effects (modulations in γ due to quiver motion) or density fluctuations (modulations in n due to plasma waves).

From Eqs. (5)–(8) it is straightforward to deduce the plasma energy balance[19]

$$\frac{\partial}{\partial t}\left[n\gamma-n_0+\frac{1}{2}\left(\frac{\partial\phi}{\partial z}\right)^2-\frac{1}{2}\Omega_p^2AA^*\right]+\frac{\partial}{\partial z}(np_z)=-\frac{1}{2}\frac{\partial\Omega_p^2}{\partial t}AA^* \tag{10}$$

and momentum balance

$$\frac{\partial}{\partial t}(np_z)+\frac{\partial}{\partial z}\left[nv_zp_z-n_0\phi-\frac{1}{2}\left(\frac{\partial\phi}{\partial z}\right)^2+\frac{1}{2}\Omega_p^2AA^*\right]=\frac{1}{2}\frac{\partial\Omega_p^2}{\partial z}AA^*. \tag{11}$$

The $\Omega_p^2AA^*$ term has been included in the l.h.s. of the equations to explicitly show the energy and momentum conservation, as the r.h.s. now exactly balances to 0 after adding Eqs. (3) and (4).

A useful reduction of the fluid model is the quasistatic approximation, which consists of replacing the full (z,t) dependence of all plasma quantities with a dependence on $\zeta=z-t$ only. This means that each element of the plasma electron fluid responds in the same way to the laser pulse as it passes by. This approximation is only valid if changes to the pulse envelope AA^* can be neglected during the time it takes the laser pulse to propagate a distance equal to its own length, i.e. if the envelope evolves slowly in the co-moving frame. This property is consistent with the separation of time scales on which photon kinetic theory is built. The quasistatic approximation leads to the relation $\gamma-p_z=1+\phi$, which enables all plasma quantities to be expressed in terms of AA^* and ϕ, for example,

$$\gamma=\frac{1}{2}\left(1+\phi+\frac{1+AA^*}{1+\phi}\right),\quad \Omega_p^2=\frac{\omega_p^2}{1+\phi}. \tag{12}$$

Due to the identification $\partial/\partial\zeta=\partial/\partial z=-\partial/\partial t$, Eqs. (10) and (11) reduce to a single expression

$$\frac{\partial}{\partial\zeta}\left[\frac{1}{2}\left(\frac{\partial\phi}{\partial\zeta}\right)^2+\frac{1}{2}\Omega_p^2\phi^2\right]=-\frac{1}{2}\frac{\partial\Omega_p^2}{\partial\zeta}AA^*, \tag{13}$$

which follows from the quasistatic equation

$$\frac{\partial^2\phi}{\partial\zeta^2}=\frac{\omega_p^2}{2}\left[\frac{1+AA^*}{(1+\phi)^2}-1\right]. \tag{14}$$

Notice that the kinetic and potential energy of the plasma, which is the quantity in the square brackets on the l.h.s. of Eq. (13), has a natural interpretation as the Hamiltonian of an anharmonic oscillator with coordinate ϕ, velocity $\partial\phi/\partial\zeta$, frequency Ω_p.[20] The oscillation is of course simply a plasma wave, driven by the laser pulse ponderomotive force. The anharmonicity is due to the dependence of the frequency Ω_p on the coordinate ϕ. Equation (13) shows that the Hamiltonian is constant in regions where $AA^*=0$, i.e., both behind and in front of the laser pulse. As we would expect, the difference in the value of the Hamiltonian on both sides of the laser pulse is equal to the rate of energy transfer between the laser pulse and the plasma.

IV. PHOTON KINETIC THEORY

In this section, we present a derivation of the photon Vlasov equation, which closely follows Ref. 9. Subsequently, we briefly discuss the absence of phase information in photon kinetic theory and reconstruct the conservation laws given in Sec. II. We start our derivation by defining the following Wigner transform:

$$\mathcal{A}(z,t,k,\omega) = \int dsd\tau \exp(i\omega\tau - iks) \times A(z+s/2, t+\tau/2)A^*(z-s/2, t-\tau/2). \quad (15)$$

The dependence on (z,t) is assumed to describe the slow evolution of the amplitude of the laser pulse, while the (k,ω) dependence describes the fast high frequency spectral content of the pulse. The dependence on both ω and t allows easy representation of correlations between temporal and spectral pulse features (i.e., frequency chirp). From the wave equation (1), it can be deduced that $\mathcal{A}$ obeys

$$\omega\frac{\partial\mathcal{A}}{\partial t} + k\frac{\partial\mathcal{A}}{\partial z} = \Omega_p^2 \sin\Lambda\mathcal{A}, \quad (16)$$

where Λ operates to the left and the right on two different functions

$$P\Lambda Q = \frac{\partial P}{\partial z}\frac{\partial Q}{\partial k} - \frac{\partial P}{\partial t}\frac{\partial Q}{\partial \omega}, \quad (17)$$

the sine of the operator is to be understood as a Taylor expansion

$$\sin\Lambda = \sum_{n=0}^{\infty}\frac{1}{(2n+1)!}\Lambda^{2n+1}, \quad (18)$$

and powers of Λ are defined with binomial coefficients

$$P\Lambda^n Q = \sum_{m=0}^{n}\binom{m}{n}(-)^m\frac{\partial^n P}{\partial z^{n-m}\partial t^m}\frac{\partial^n Q}{\partial k^{n-m}\partial\omega^m}. \quad (19)$$

These definitions follow naturally from the Taylor expansion of $\Omega_p^2(z\pm s/2, t\pm\tau/2)$ around $s=0$, $\tau=0$. The information contained in $\mathcal{A}$ includes for example the envelope of the laser pulse

$$AA^*(z,t) = \int\int \mathcal{A}(z,t,k,\omega)dkd\omega \quad (20)$$

and the envelope of the double Fourier transform $\hat{A}$

$$\hat{A}\hat{A}^*(k,\omega) = \int\int \mathcal{A}(z,t,k,\omega)dzdt. \quad (21)$$

Integration of Eq. (16) yields the following conservation law:

$$\frac{\partial}{\partial t}\int\int \omega\mathcal{A}dkd\omega + \frac{\partial}{\partial z}\int\int k\mathcal{A}dkd\omega = 0, \quad (22)$$

which is equivalent to the conservation of wave action. Thus $\omega\mathcal{A}$ can be interpreted as a photon phase space density f_p in an extended phase space (k,z,ω). However, note that Eq. (16) is not a proper Vlasov equation for f_p, because Liouville's theorem does not apply here. For example, Eq. (16) would allow regions of negative phase-space density to develop from initial conditions with strictly positive values of f_p.

To arrive at a proper Vlasov equation for quasiparticles from Eq. (16), two approximations are needed, which have far-reaching consequences. The first approximation is to drop all higher-order terms in Λ, which amounts to neglecting all interference and higher order dispersion effects. This effectively turns the wave theory into a particle theory, as we can now define the characteristics along which $\omega\mathcal{A}$ is transported, i.e. the equations of motion for the quasiparticles

$$\frac{dz}{dt} = \frac{k}{\omega}, \quad \frac{dk}{dt} = -\frac{1}{2\omega}\frac{\partial\Omega_p^2}{\partial z}, \quad \frac{d\omega}{dt} = \frac{1}{2\omega}\frac{\partial\Omega_p^2}{\partial t}. \quad (23)$$

These equations are easily recognized as ray-tracing equations.

The second approximation is that of geometrical optics and involves the introduction of a local dispersion relation, i.e., an expression of ω as a prescribed function $\Omega(k,z,t)$. The appropriate relation for photons in a plasma is

$$\Omega^2 = k^2 + \Omega_p^2(z,t), \quad (24)$$

which is similar to the relation between energy and momentum for a relativistic particle. This naturally leads to the identification of frequency Ω with the energy and wave number k with the momentum of a single photon, just as in quantum mechanics. In addition, photons in a plasma are seen to have an effective mass m_p, given by $m_p c^2 = \hbar\Omega_p$ (in dimensional units). Thus the "photons" in photon kinetic theory are "dressed"[21] in the sense that they contain a mixture of electromagnetic and plasma degrees of freedom. The identification of Ω with energy also explains the use of the terms "photon acceleration"[22] and "photon deceleration" for describing the adiabatic blueshift or redshift due to slow temporal variations of the medium. The frequency Ω plays the role of the Hamiltonian with canonical coordinates (k,z). The Hamiltonian equations are identical to (23), with ω replaced by Ω, e.g., the photon velocity k/ω is equal to the group velocity $\partial\Omega/\partial k$. Finally, a proper Vlasov equation for the photon density $f_p(k,z,t)$ is found

$$\frac{\partial f_p}{\partial t} + \frac{\partial f_p}{\partial z}\frac{\partial\Omega}{\partial k} - \frac{\partial f_p}{\partial k}\frac{\partial\Omega}{\partial z} = \frac{\partial f_p}{\partial t} + [f_p,\Omega] = 0. \quad (25)$$

The evolution of f_p according to this Vlasov equation excludes a correct treatment of interference effects. A simple example might be helpful to illustrate this point. Consider a monochromatic standing wave in vacuum, described by $A(z,t) = A_0\exp[i\omega_0(t-z)] + A_0\exp[i\omega_0(t+z)]$. The Wigner transform is given by

$$\mathcal{A}(z,t,k,\omega) = A_0^2\delta(\omega-\omega_0) \times[\delta(k-\omega_0) + \delta(k+\omega_0) + 2\cos(2\omega_0 z)\delta(k)], \quad (26)$$

which can be interpreted as a photon distribution consisting of three separate groups, two describing the left and right-propagating waves and one describing their standing wave interference pattern. The "propagating photons" obey the vacuum dispersion relation $\omega=k$, while the "standing photons" do not $(\omega=\omega_0\neq 0=k)$. In general, interference between two wave packets involves such a third group of photons, which one might call a cloud of "virtual photons" that only exists where and when the two wave packets overlap in space and time. If the wave packets happen to overlap at $t=0$, it is straightforward to include the third group of photons in the initial distribution (note that this may involve

regions of negative phase-space density). However, the evolution of this third photon group will not, in general, be correctly reproduced with Eq. (25), because the dispersion relation (24) is imposed. Moreover, group velocity dispersion effects due to photon acceleration and deceleration can cause different parts of a single wave packet, which were not overlapping at $t=0$, to overlap at some $t>0$ with different wave numbers. This would also give rise to interference, and cannot be reproduced if one starts with the single wave packet and evolves it according to (25). A proper description of this effect would require dropping the first approximation ($\sin\Lambda\approx\Lambda$) as well, because regions of negative phase-space density might have to evolve from initial conditions with strictly positive values of f_p. The exclusion of interference in photon kinetic theory is in line with the absence of phase information: only envelope quantities like AA^* can be reconstructed from the photon density f_p.

The conservation of wave action, or conservation of photon number,

$$\frac{\partial}{\partial t}\int f_p dk+\frac{\partial}{\partial z}\int \frac{kf_p}{\Omega}dk=0, \tag{27}$$

is integral to the photon kinetic theory. The conservation of photon number implies that a pulse that loses energy in a plasma will experience redshift, as individual photons can lose energy only by photon deceleration. The situation is different for a laser pulse that propagates in a gas and (partly) ionizes the medium. It is experimentally well established that the pulses lose energy to an ionization front, while at the same time experiencing frequency blueshift. Clearly, in this case the number of photons is not conserved.

From the identification of Ω with energy, k with momentum and k/Ω with velocity, it is straightforward to derive expressions for the conservation of energy:

$$\frac{\partial}{\partial t}\int \Omega f_p dk+\frac{\partial}{\partial z}\int kf_p dk=\frac{1}{2}\frac{\partial\Omega_p^2}{\partial t}\int\frac{f_p}{\Omega}dk, \tag{28}$$

and the conservation of momentum:

$$\frac{\partial}{\partial t}\int kf_p dk+\frac{\partial}{\partial z}\int\frac{k^2f_p}{\Omega}dk=-\frac{1}{2}\frac{\partial\Omega_p^2}{\partial z}\int\frac{f_p}{\Omega}dk. \tag{29}$$

The photon energy density and momentum flux are seen to contain the previously mentioned $\Omega_p^2AA^*$ contributions, which are associated with the energy of plasma quiver motion. This reflects the dressed character of the photons, i.e., the fact that they contain both electromagnetic and plasma degrees of freedom, and explains why it is natural to include these terms on the l.h.s. of Eqs. (3), (4), (10), and (11). Including the electron quiver energy in the photon description effectively separates the fast and slow time scales, as the photon energy density only contains contributions from the fast time scale (f_p or A), while the plasma energy density in Eq. (13) can be written in terms of the slow plasma quantities ($\phi,\partial\phi/\partial\zeta$) exclusively. The two are coupled through the slowly varying envelope AA^* and the slow space and time variations of Ω_p^2.

V. SIMULATION RESULTS

In this section, we briefly sketch the full wave and photon kinetic algorithms and present simulation results. To model the slow plasma response, both codes solve Eq. (14) on a numerical grid with a second order finite-difference method. The full wave code solves Eq. (1) numerically on the same grid with a method based on the Green's function for the one-dimensional wave equation, treating Ω_p^2A as a source term (emission of transverse waves by the plasma electrons). The general solution to the homogeneous wave equation consists of two arbitrary functions, both of which propagate at the speed of light, one to the left and one to the right. The straightforward implementation of this is to split A in its right and left-propagating parts, which are shifted by one grid cell at each time step (this assumes the time sampling interval equal to the grid spacing in $c=1$ units). The Green's function is equal to $-1/2$ in the light cone forward from the source point (z_s,t_s), and equal to 0 elsewhere in space and time. This solution can be rewritten as a series of signals that emanate from z_s and propagate to the left and to the right at the speed of light, at all times $t>t_s$. Again, the propagation of the signals is done by cell-shifting, while a separate variable is used to determine the weight of the signals emitted from each point on the space grid at each time step. This weight, which is actually the time-integrated current density at z_s, is updated by adding new contributions at each time step: there is no need to keep the time history of the system. This implementation of the wave equation is just as efficient as the usual finite-difference time domain integration.

The numerical solution to the photon Vlasov equation (25) is implemented using the particle-in-cell approach,[11] which in this case can be called a "photon-in-cell" method. Simulation particles are pushed forward in time by a fourth order Runge-Kutta algorithm for the equations of motion (23), solving only for z and k, while Ω is derived from the dispersion relation (24). Calculation of AA^* on the grid and evaluation of $\partial\Omega_p^2/\partial z$ at the particle location are done with second order projection and interpolation methods. Before calculating the potential ϕ, filtering is applied to AA^* to reduce the particle noise. This particle noise gives rise to a spurious, noisy ponderomotive force which may drive local numerical instabilities.

The initial laser field is $A(\zeta)=A_0\exp(i\omega_0\zeta-\zeta^2/L^2)$, where $A_0=1$ is the amplitude, $\omega_0=20\omega_p$ is the optical frequency and the pulse length L is given by $\omega_pL=16$ or 2 for the long and short pulse cases, respectively. The initial photon distribution corresponding to the laser field is approximated with the following the spatial Wigner transform $f_p(\zeta,k)=\omega_0\int A(\zeta+s/2)A^*(\zeta-s/2)\exp(-iks)ds$. To define a convenient time unit for the long-term interaction, we introduce $\omega_e=\omega_p^3/\omega_0^2$. We compare the evolution of the envelope $AA^*=\int(f_p/\Omega)dk$ and the Fourier spectrum $\hat{A}\hat{A}^*=\int(f_p/\Omega)d\zeta$, in both codes, where $\hat{A}$ denotes the spatial Fourier transform of A.

We first discuss the evolution of the long pulse, whose initial conditions are represented in Fig. 1. The plasma response, as given by Ω_p^2, confirms our earlier statement that

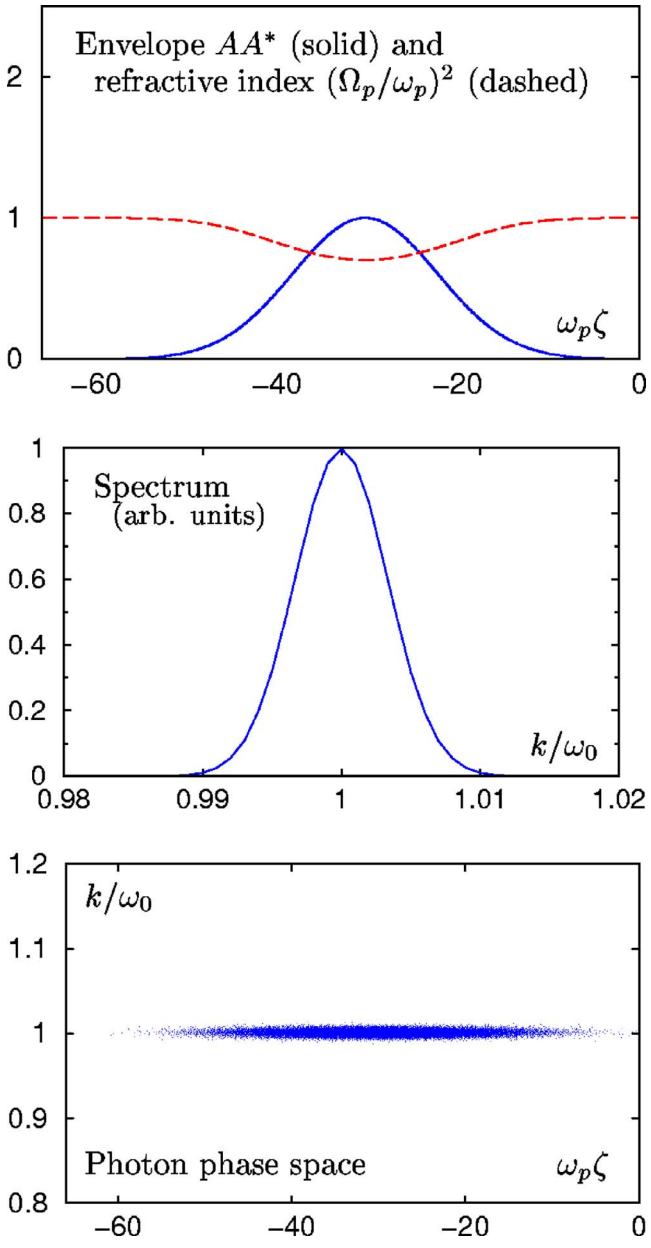

FIG. 1. (Color online) Snapshot of long pulse simulation at $t=0$.

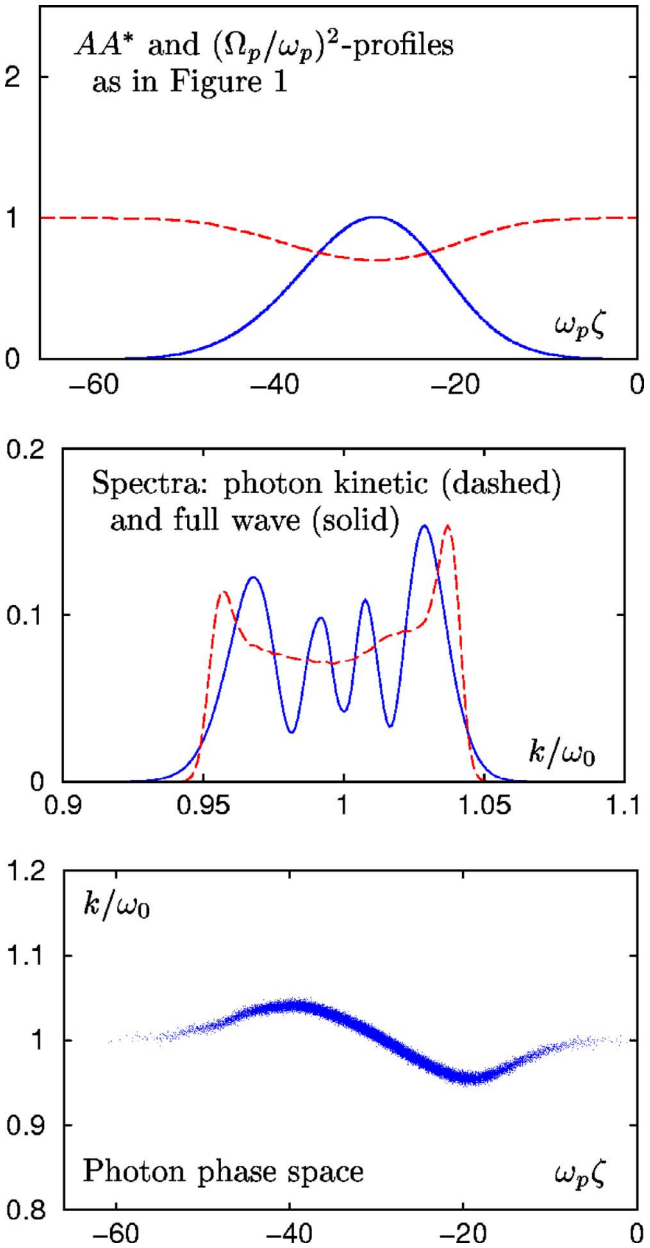

FIG. 2. (Color online) Snapshot of long pulse simulation at $\omega_e t=4$.

there is no wakefield initially. The dip in the Ω_p^2 profile inside the laser pulse is a purely relativistic effect, caused by the quiver motion, which changes γ and consequently also $\Omega_p^2 \propto n/\gamma$. At this stage of the simulation, we have applied sufficient Fourier filtering to the photon kinetic AA^* profile in order to suppress spurious wakefield excitation from the particle noise, which would form a numerical seed for the self-modulation instability.

At time $\omega_e t=4$, the envelope profiles from both codes are still indistinguishable, as shown in Fig. 2. The Ω_p^2 profile shows that the wakefield has not yet developed at this stage, implying no net energy exchange between the plasma and the laser pulse has taken place. The scatter plot of the photon phase space at $\omega_e t=4$ shows that energy has been transferred locally within the pulse, as photons have been decelerated in the front part and accelerated in the rear part. As a consequence, the peak of the envelope has moved forward and the front of the pulse has steepened, which can be understood by recalling that AA^* is proportional to $1/\Omega$. This steepening forms the physical (rather than numerical) seed from which the self-modulation instability will grow. In agreement with the photon acceleration and deceleration, both codes show a spectrum that is broader than the initial spectrum, with a peak on either side. The difference is that the photon kinetic code has a nearly flat region in between the peaks, where the full wave code spectrum shows oscillatory behavior.

The third time snapshot of the long pulse evolution, shown in Fig. 3, is taken at $\omega_e t=8$. The shape of the pulse envelope and the plasma response from both codes are still in good agreement. By now, pulse deformation has become more pronounced and a small amplitude wakefield is excited. The small amplitude pulse envelope oscillations visible in the photon kinetic simulation result are due to particle noise.

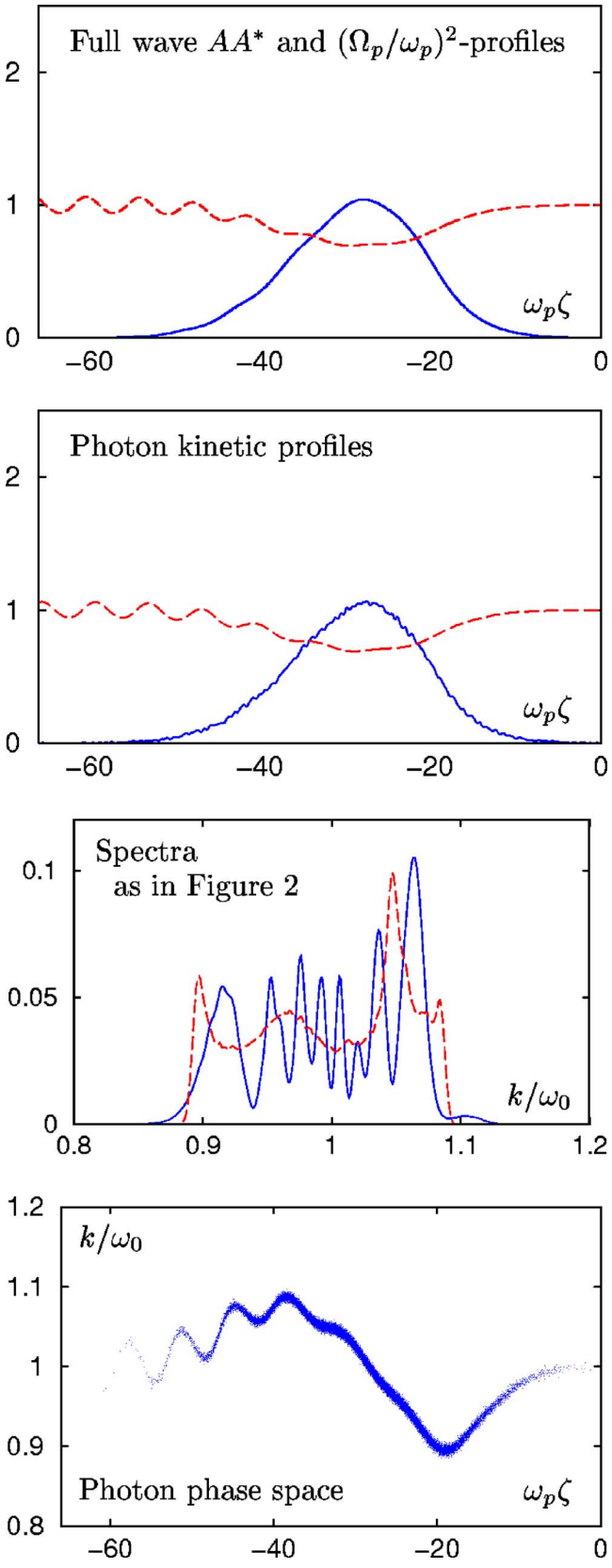

FIG. 3. (Color online) Snapshot of long pulse simulation at $\omega_e t=8$.

At this stage of the simulation, we have relaxed the Fourier filtering to avoid oversmoothing the AA^* profile. The photon phase space plot shows the initial stage of self-modulation, as the photon energy is being modulated at the plasma wavelength in the rear part of the pulse. In agreement with this, both Fourier spectra show multiple peaks, as the modulation leads to photon bunching around certain k values. The difference between the spectra is as before, with the full wave spectrum showing more oscillations.

The last snapshot of the long pulse evolution, which shows the self-modulation in its full glory, is taken at $\omega_e t=12$ and shown in Fig. 4. The codes now produce different profiles for AA^* and Ω_p^2, especially at the rear of the pulse. This can be understood from inspection of the phase space scatter plot, which shows that photons are dramatically decelerated in the rear part, to the point that their frequency starts to approach the (local) plasma frequency Ω_p. This limit is beyond the validity of photon kinetic theory, which is built on a clear separation between plasma and optical time scales. Consequently, we cannot expect full quantitative agreement between the full wave and photon kinetic simulations. It is interesting to note that the slowly varying amplitude approximation breaks down in the same limit $\Omega \to \Omega_p$.

Interesting qualitative aspects of the evolution can be interpreted by comparing the full wave and photon kinetic simulation results. As an example, consider the feature around $\omega_p\zeta=-55$ in the full wave AA^* profile, which shows a short wavelength envelope modulation. Inspecting the corresponding group of photons in the phase space scatter plot, we find that part of the photon distribution has "folded," so that two groups of photons with very different k values can be found at the same coordinate ζ. This "folding" is precisely the type of evolution we have mentioned above, when group velocity dispersion effects due to photon acceleration and deceleration cause different parts of a single wave packet, which were not overlapping at $t=0$, to overlap at some $t>0$ with different wave numbers and thus cause interference. In our interpretation, the short wavelength envelope modulation found in the full wave code is the beat wave pattern associated with this interference.

The Fourier spectra corresponding to $\omega_e t=12$ exhibit the same differences that we have noted before and are shown to illustrate that a remarkable qualitative agreement is maintained even when the self-modulation instability has fully developed. From the phase space scatter plot, individual peaks in the photon kinetic spectrum are easily linked to particular positions within the pulse (usually corresponding to a minimum in Ω_p^2) where photon k bunching has taken place.

Unlike the case of the long pulse, several authors have discussed the short pulse evolution in photon kinetic terms before.[23,24] We give a brief summary of this discussion here, followed by some comments specific to our simulation results. As expected for short pulses, almost all photons are located within the first half of the first plasma wave bucket, where they undergo photon deceleration and lose energy to the wakefield. Consequently, a large drop in average frequency occurs, as seen in the Fourier spectra in Fig. 5, which represent the initial spectrum and snapshots at $\omega_e t=3.6$. The photon deceleration is accompanied by amplitude increase of the vector potential envelope and the formation of a large spike at the rear part of the pulse, as is visible in the AA^* profiles. The increase and steepening of AA^* is a result of

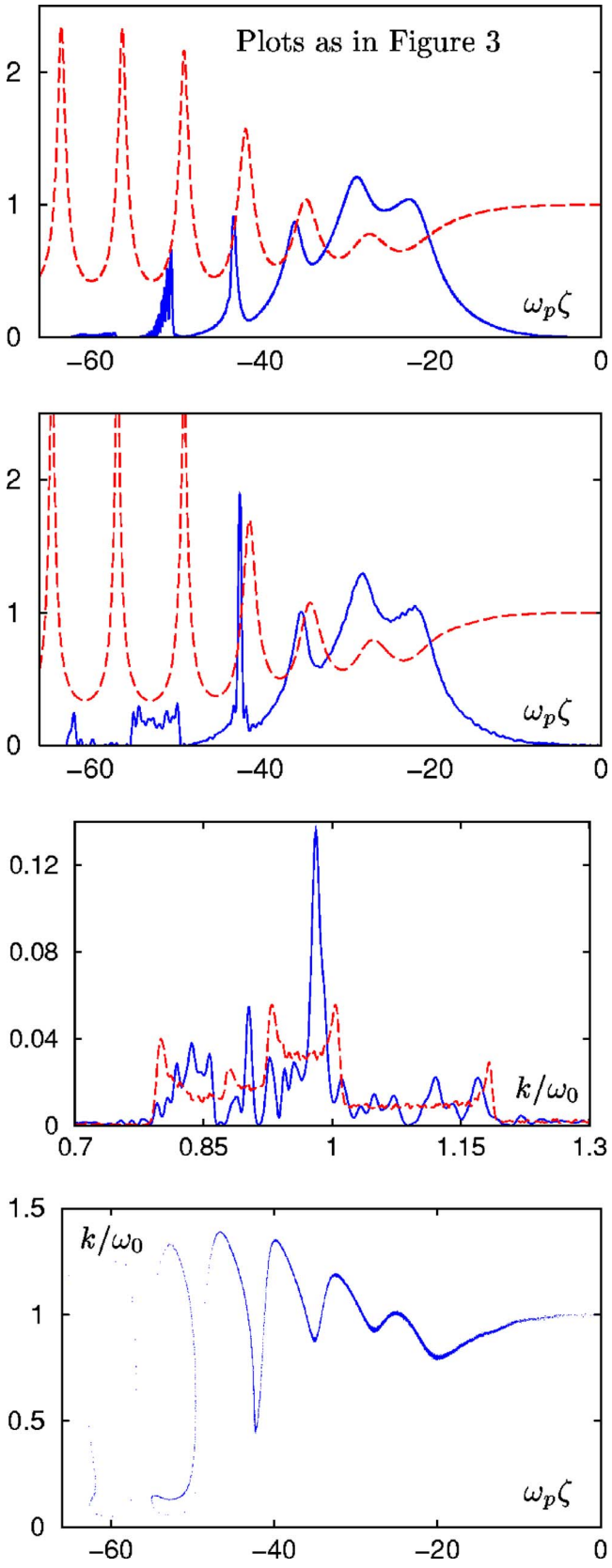

FIG. 4. (Color online) Snapshot of long pulse simulation at $\omega_e t = 12$.

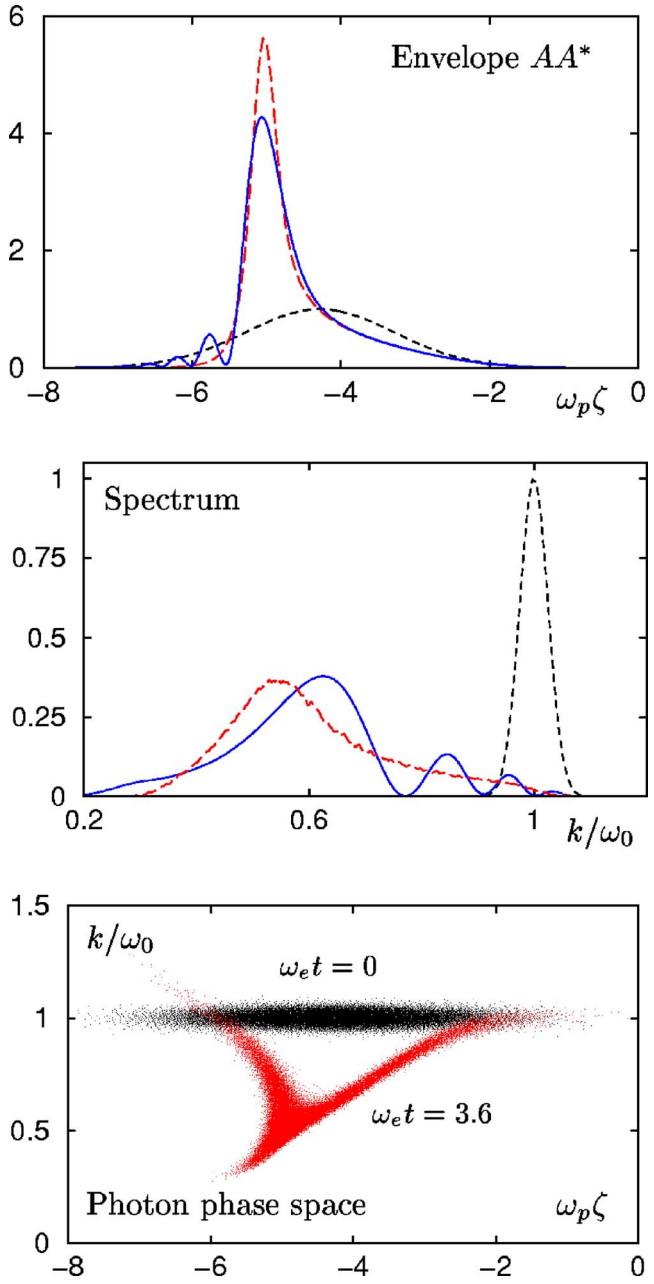

FIG. 5. (Color online) Short pulse simulation: in the envelope and spectrum plots, the dotted lines represent the initial conditions, the solid lines show the full wave result at $\omega_e t = 3.6$, and the dashed lines correspond to the photon kinetic result at $\omega_e t = 3.6$.

both photon deceleration and group velocity dispersion. As $AA^* \propto f_p/\Omega$, a drop in frequency corresponds to an increase of the vector potential amplitude, which subsequently leads to a stronger ponderomotive force and a larger wakefield amplitude. Consequently, the transfer of energy from laser pulse to plasma is enhanced and the photon deceleration speeds up. This feedback loop leads to an explosive instability with a time dependence of the average frequency proportional to $(1-t/t_N)^{1/3}$.[25] The typical time scale t_N is proportional to $1/(\omega_e U_0)$, where U_0 is the initial pulse energy. As the frequency drop is nonuniform along the length of the pulse, different parts of the pulse have different group velocities. This leads to group velocity dispersion and, ultimately, to strong longitudinal pulse compression (photon bunching) at the rear of the pulse, as is visible in the photon phase space snapshot at $\omega_e t = 3.6$.

As the laser pulse drives a wakefield during all of its

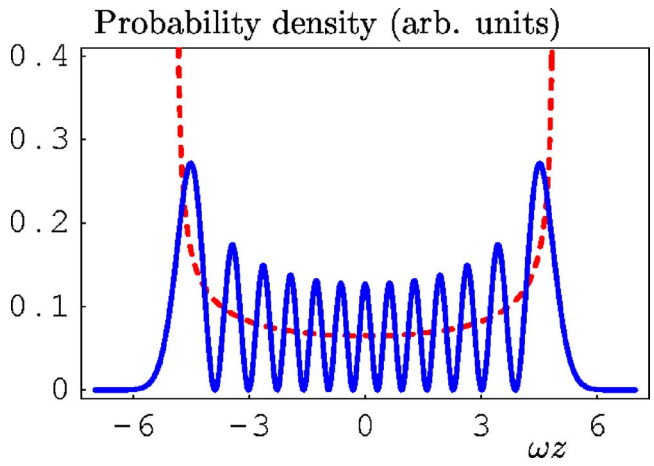

FIG. 6. (Color online) Quantum-mechanical probability density $\psi\psi^*$ in the solid line and corresponding projected classical phase space density in the dashed line, for the $n=12$ eigenstate of the harmonic oscillator.

interactions with the plasma, we have not applied Fourier filtering in the photon kinetic code to suppress spurious wakefields: a simple digital filter was sufficient to suppress excessive particle noise. The photon kinetic result is seen to overestimate the steepening of the pulse, while it fails to reproduce the short-wavelength modulation at the rear part of the pulse. We have checked that this failure is not due to the numerical grid being too coarse. Inspection of the scatter plot shows a folding of the photon phase space similar to the one discussed above, so we interpret this modulation as a beat wave pattern.

VI. DISCUSSION

To appreciate the relation between full wave and photon kinetic simulation results, note that the transition from full wave to photon kinetic theory is mathematically equivalent[26] to transforming the Schrödinger equation that describes the evolution of the wave function $\psi(z,t)$ of a particle in a potential $V(z,t)$

$$i\frac{\partial\psi}{\partial t} = -\frac{\partial^2\psi}{\partial z^2} + V\psi \tag{30}$$

into a classical Vlasov equation for the phase space density f

$$\frac{\partial f}{\partial t} + [f,\mathcal{H}] = 0, \tag{31}$$

where $\mathcal{H}(p,z,t)=p^2/2+V(z,t)$ is the Hamiltonian. The correspondence is $\psi\psi^*(z,t)\rightarrow\int f(p,z,t)dp$, etc. This transition involves the same approximations that have been presented in Sec. IV, where the photon Vlasov equation (25) is derived. With this analogy in mind, it is not difficult to understand why the photon kinetic theory does not include interference effects. Interference is also the explanation of the differences between the full wave and photon kinetic Fourier spectra, which are reminiscent of the differences between $\psi\psi^*$ profiles of eigenstates of the quantum harmonic oscillator ($V=\omega^2z^2/2$) and the projected density of corresponding classical orbits, as depicted in Fig. 6. The nth quantum eigenstate is a standing wave pattern with n nodes, which explains the oscillations in $\psi\psi^*$ as quantum interference. In contrast, the projected classical phase space density is nonzero in the whole region of the classical orbit (and singular at the turning points). After averaging over the space scale of the oscillation, the quantum profiles converge to the classical result in the limit of large quantum numbers. The agreement is lost in the opposite limit of small quantum numbers, in line with our observation that photon kinetic theory breaks down in the low-frequency limit $\Omega\rightarrow\Omega_p$.

Although interference effects are not included in photon kinetic theory, the photon phase space pictures are actually very helpful in predicting where and when these effects will occur. We have illustrated this when we discussed Fig. 4, where we have used the photon kinetic results to interpret an envelope modulation found in the full wave code as a beat wave pattern. In principle, the same information can be extracted by applying the Wigner transform to the full wave simulation results. However, in practice it can be computationally costly to calculate these Wigner transforms. More importantly, the full wave Wigner transforms contain all higher order dispersion effects and are more difficult to interpret than the simple particle picture used in photon kinetic theory.

A comparison between one-dimensional photon kinetic and slowly varying envelope codes has been reported by us in Ref. 27. It was found that the slowly varying envelope code requires much smaller grid size and time step than the photon kinetic code, and is therefore slower. Both codes give identical results for the spatial envelope until they reach the limit of validity of the underlying approximations.

Finally, we note that extension of the photon kinetic model to multidimensional geometry is straightforward from a numerical point of view. We are currently developing multidimensional photon kinetic codes and preliminary results show at least qualitative agreement between simulation results based on photon kinetic and slowly varying envelope methods.

In conclusion, we have studied laser pulse propagation in underdense plasmas with two different one-dimensional codes for two laser pulse lengths that are relevant to the ongoing development of laser wakefield accelerators. The first code is based on the full wave theory and has been used to benchmark the second one, which is based on photon kinetic theory and represents the electromagnetic field as a number of quasiparticles in coordinate-wave number phase space. This "photon-in-cell" code is able to reproduce the evolution of the full wave spatial envelope accurately until the photon frequency starts to get close to the (local) plasma frequency. This is expected, as photon kinetic theory starts to lose its validity in this regime. The Fourier spectra from the two codes agree qualitatively, and the differences can be understood from the fact that photon kinetic theory does not include interference effects, as the relation between photon kinetic theory and the full wave description is formally equivalent to the relation between the classical and quantum descriptions of particle dynamics (and classical particles do not interfere). In spite of this, the phase space pictures from the photon kinetic code clearly indicate where and when interference effects occur. This is a good example of the syn-

ergy between the full wave and photon kinetic approaches, as one is more complete and the other is more intuitive.

This work has been supported by the Research Councils of the UK under the Alpha-X programme.[28]

[1] D. Umstadter, S.-Y. Chen, A. Maksimchuk, G. Mourou, and R. Wagner, Science **273**, 472 (1996).
[2] E. Esarey, P. Sprangle, J. Krall, and A. Ting, IEEE Trans. Plasma Sci. **24**, 252 (1996).
[3] K. W. D. Ledingham, AIP Conf. Proc. **634**, 123 (2002).
[4] D. A. Jaroszynski and G. Vieux, AIP Conf. Proc. **647**, 902 (2002).
[5] W. L. Kruer and S. C. Wilks, AIP Conf. Proc. **314**, 16 (1992).
[6] S. W. McDonald and A. N. Kaufman, Phys. Rev. A **32**, 1708 (1985).
[7] E. P. Wigner, Phys. Rev. **40**, 749 (1932).
[8] W. Heisenberg, Phys. Z. **32**, 737 (1931).
[9] N. L. Tsinstadze and J. T. Mendonça, Phys. Plasmas **5**, 3609 (1998).
[10] L. Oliveira e Silva and J. T. Mendonça, Phys. Rev. E **57**, 3423 (1998).
[11] C. K. Birdsall and A. B. Langdon, *Plasma Physics via Computer Simulation* (Adam Hilger, Bristol, 1991).
[12] C. S. Liu, M. N. Rosenbluth, and R. B. White, Phys. Fluids **17**, 1211 (1974).
[13] C. J. McKinstrie and R. Bingham, Phys. Fluids A **4**, 2626 (1992).
[14] A. Ting, E. Esarey, and P. Sprangle, Phys. Fluids A **2**, 1390 (1990).
[15] C. Labaune, S. Baton, T. Jalinaud, H. A. Baldis, and D. Pesme, Phys. Fluids A **4**, 2224 (1992).
[16] T. Tajima and J. M. Dawson, Phys. Rev. Lett. **43**, 267 (1979).
[17] R. A. Cairns, A. Reitsma, and R. Bingham, Phys. Plasmas **11**, 766 (2004).
[18] P. Sprangle, E. Esarey, and A. Ting, Phys. Rev. A **41**, 4463 (1990).
[19] A. J. Brizard, J. Plasma Phys. **71**, 225 (2005).
[20] R. M. G. M. Trines, V. V. Goloviznin, L. P. J. Kamp, and T. J. Schep, Phys. Rev. E **63**, 026406 (2001).
[21] J. C. Garrison and R. Y. Chiao, Phys. Rev. A **70**, 053826 (2004).
[22] S. C. Wilks, T. Katsouleas, and J. M. Dawson, AIP Conf. Proc. **193**, 448 (1989).
[23] D. F. Gordon, B. Hafizi, R. F. Hubbard, J. R. Penano, P. Sprangle, and A. Ting, Phys. Rev. Lett. **90**, 215001 (2003).
[24] A. J. W. Reitsma, R. A. Cairns, R. Bingham, and D. A. Jaroszynski, Phys. Rev. Lett. **94**, 085004 (2005).
[25] S. V. Bulanov, I. N. Inovenkov, V. I. Kirsanov, N. M. Naumova, and A. S. Sakharov, Phys. Fluids B **4**, 1935 (1992).
[26] S. W. McDonald, Phys. Rev. A **43**, 4484 (1991).
[27] A. J. W. Reitsma and D. A. Jaroszynski, AIP Conf. Proc. **737**, 771 (2004).
[28] http://phys.strath.ac.uk/alpha-x/